Charge correlations in polaron hopping through molecules

Benjamin B. Schmidt,[1,2] Matthias H. Hettler,[2] and Gerd Schön[1,2]

[1]*Institut für Theoretische Festkörperphysik und DFG Center for Functional Nanostructures (CFN),
Karlsruhe Institute of Technology, 76128 Karlsruhe, Germany*

[2]*Institut für Nanotechnologie, Karlsruhe Institute of Technology, 76344 Eggenstein-Leopoldshafen, Germany*

In many organic molecules, the strong coupling of excess charges to vibrational modes leads to the formation of polarons, i.e., localized states of charge carriers and molecular deformations. At room temperature, incoherent hopping of polarons along the molecule is the dominant mechanism of charge transport. We study the situation far-from-equilibrium where, due to an applied voltage bias, the induced number of charge carriers on the molecule is high and charge correlations become relevant. We develop a diagrammatic theory that accounts in a finite system for all many-particle correlations and their effect on the incoherent transport. We determine the *I-V* characteristics of short sequences of DNA by expanding the diagrammatic theory up to second order in the hopping parameters. Correlations qualitatively modify the results as compared to those obtained in a mean-field approximation.

I. INTRODUCTION

Molecular electronics experiments performed during recent years have probed the conductance and current-voltage characteristics of a large variety of molecules. Several experiments on long molecules indicate that transport is not described by coherent Landauer transport or tunneling but rather by an incoherent hopping of charge carriers along the molecule. Examples are experiments on DNA (Refs. [1] and [2]) or oligophenyleneimine wires.[3] In the latter experiment, the length dependence of the conductance clearly demonstrated the crossover from the coherent (tunneling) to the incoherent transport regime at a molecule length of about 4 nm.

In many experiments, the molecule consists of repeated segments (either identical or with chemical modifications) where the quantum-mechanical hopping amplitude between the segments can be tuned to some degree by the choice of the "linker group." If the hopping amplitude between the segments is large (e.g., for stiff molecules with fully conjugated electron systems) the quantum-mechanical coherence on the molecule can extend quite far at low temperatures, such that even molecules of up to several nanometer length display signs of coherent transport, at least within the molecule.[4,5] On the other hand, if the coupling of segments is weak (e.g., for flexible molecules with weakly conjugated or saturated linker groups) the coherence decays quickly, such that charge carriers are typical localized over a single or a few segments only. In this case, the molecule tends to change its conformation in order to lower its energy when charged, a process called polaron formation. The polaron is a combination of a charge carrier and the localized deformation. At room temperature, charge transport is then dominated by incoherent hopping of polarons along the molecule. At low temperature, coherent "bandlike" transport of polarons might be observable.

The theoretical description of polaronic effects in molecule-electrode setups so far either focused on molecular single-level systems[6–9] or described polaron hopping in long molecules by assuming "simple" rate equations.[10,11] Böttger

and Bryksin have shown in a rigorous description of polaron transport in bulk systems that even in the absence of Coulomb interactions phonon-mediated charge correlations between different sites develop.[12] However, in their calculations they included these correlations only in a mean-field like manner. The earlier rate equation approaches to polaron hopping in nanoscale systems also treat correlations within this mean-field approximation.

The mean-field approximation to many-particle correlations can be justified in systems with low density of charge carriers, and is a sufficient approximation for many doped (organic) semiconductors. In molecular electronics experiments, however, where a transport bias on the order of 1 V is applied over a molecule of a few nanometer length, the average charge density may be much higher, and correlations become relevant. For example, for small molecules often the Coulomb interaction (or charging energy) dominates, leading at low temperatures to transport characteristics similar to single-electron transistors.[13,14] With increasing molecule size, the relevance of Coulomb blockade decreases, but still, the transport *along* the molecule is affected by charge correlations, either due to (nonlocal) Coulomb interaction or the (retarded) interactions mediated by the coupling of charge carriers to vibrational modes mentioned above. We will demonstrate that in general such correlations are not sufficiently described by a mean-field approach.

We have extended the diagrammatic approach by Boettger and Bryksin to describe molecular systems coupled to metallic electrodes. In the usual diagrammatic approach to small molecules (or quantum dots),[15,16] the molecular *eigenstates* including the Coulomb interaction are the basis of a perturbative expansion in the weak coupling to metallic electrodes. In contrast, in the present problem the "basis states" are "local" to the molecule segments (e.g., a DNA base pair or a phenylene ring). The expansion parameters also include the small hopping amplitudes between the molecular segments. As the perturbation expansion usually involves a "self-energy" resummation, where diagrams of a certain type (but of arbitrarily high order) are accounted for, the occupation numbers (or, in general, one-particle correlation functions)
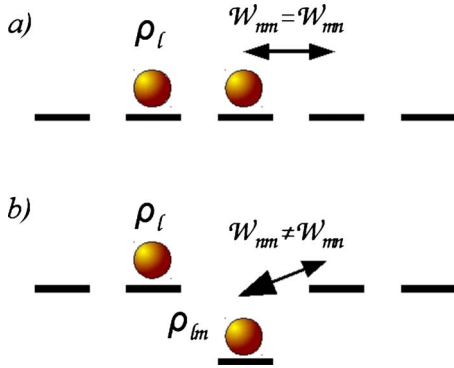
FIG. 1. (Color online) Sketch of charge carriers, hopping rates, and correlations. (a) On a homogeneous chain the rates $\mathcal{W}_{nm}$ are all equal. The occupations ρ_l are independent of the two-particle correlations ρ_{lm} as the corresponding terms in the rate equation cancel out, cf. Eq. (14). (b) On an inhomogeneous chain the rates $\mathcal{W}_{nm} \neq \mathcal{W}_{mn}$ so the two-particle correlations ρ_{lm} affect the occupations ρ_l. Since the modifications do not remain local, the transport through the entire system is changed.

are coupled to higher-order correlations functions, unless the system is noninteracting. Similar to, e.g., equation-of-motion methods, a hierarchy of equations for the correlation functions can be generated, which has to be truncated in some manner (often following more numerical necessities than physical arguments).

The present paper demonstrates that an exact description of correlation effects mediated by vibrational modes is possible for a *finite-size system*. This is because the hierarchy is naturally truncated at the level of the highest possible correlation function involving all "sites" of the molecule. The resulting finite set of coupled *linear* equations for the occupation number and the many-particle correlation functions can then be solved without resorting to any further truncation procedure. The many-particle correlation functions affect the charge occupations and the transport for nonuniform systems, see Fig. 1.

As an example we study short DNA molecules coupled to metallic electrodes. The DNA is modeled by a tight-binding chain identifying each base pair with a single tight-binding site. The sites describing either guanine-cytosine (GC) or adenine-thymine (AT) base pairs have different on-site energies and are coupled by direction-(sequence-) dependent hopping integrals t_{ij} (compare Table I). The polarons are formed by strong coupling of the charge degrees of freedom

TABLE I. Hopping integrals t_{ij} taken from Ref. 25 and adapted to our model. The notation 5′-XY-3′ indicates the direction along the DNA strand [see, e.g., Fig. 1b in Ref. 24.] 5′-XY-3′(all in electron volt).

X\Y	G	C	A	T
G	0.119	0.046	−0.186	−0.048
C	−0.075	0.119	−0.037	−0.013
A	−0.013	−0.048	−0.038	0.122
T	−0.037	−0.186	0.148	−0.038

to local base pair vibrations. To ensure energy dissipation, these base pair vibrations are in turn coupled to a set of harmonic oscillators, describing the influence of a dissipative environment.

In the *first part* of this paper, we introduce the diagrammatic technique describing incoherent polaron hopping transport through molecules or other nanoscale systems which are coupled to metallic electrodes. This technique allows the description of polaron transport with the exact consideration of correlation effects arising from the electron-vibration interaction. The approximation of the technique lies in the need to restrict the order of the expansion in small hopping parameters. In the *second part*, we apply this diagrammatic technique to polaron hopping transport through short DNA molecules coupled to metallic electrodes with the following results: (i) correlations effects beyond the mean-field approximation are relevant for the linear conductance in inhomogeneous DNA molecules already for low charge densities of less than 1%. (ii) When a transport bias is applied over the molecule, correlation effects become important even when the occupation in equilibrium is negligible. (iii) Inhomogeneous DNA molecules in general exhibit two maxima in the zero-bias conductance as a function of equilibrium chemical potential (gate voltage) and also in the differential conductance as a function of applied transport bias. In contrast, the mean-field approach only displays one maximum. (iv) Depending on the sequence, the secondary maxima can be suppressed, as a consequence of a small hopping rate limiting the transport through the system. Details of the diagrammatic technique are shown in Appendices A and C.

II. MODEL AND TECHNIQUE

The minimal Hamiltonian to describe polaron transport through DNA is $H = H_{el} + H_{vib} + H_{el-vib} + H_L + H_R + H_{T,L} + H_{T,R} + H_{bath}$ with

$$H_{el} = \sum_i \hat{\epsilon}_i a_i^\dagger a_i - \sum_{\langle ij \rangle} t_{ij} a_i^\dagger a_j,$$

$$H_{T,L} + H_{T,R} = \sum_{n,r,i} [t^r c_{nr}^\dagger a_i + t^r a_i^\dagger c_{nr}],$$

$$H_{vib} = \sum_\alpha \sum_i \omega_{\alpha i} \left(B_{\alpha i}^\dagger B_{\alpha i} + \frac{1}{2} \right),$$

$$H_{el-vib} = \sum_\alpha \sum_i \lambda_{\alpha i} a_i^\dagger a_i (B_{\alpha i} + B_{\alpha i}^\dagger). \quad (1)$$

The term H_{el} models the electrons on the molecule with operators $a_i^\dagger, a_i$ in a single-orbital tight-binding representation. This implies that the molecule consists of N parts (labeled i). The electronic properties of the molecule can then be described by the molecular orbitals [usually the highest occupied molecular orbital (HOMO) or lowest unoccupied molecular orbital (LUMO)] of these subentities with on-site energies ϵ_i and hopping t_{ij} between neighboring parts of the molecule. The terms $H_{L/R}$ refer to the left and right electrodes. They are modeled by noninteracting electrons, de-

scribed by operators $c^\dagger_{n\mathrm{L/R}}, c_{n\mathrm{L/R}}$, with a flat density of states ρ_e (wide band limit) and a chemical potential $\mu_{\mathrm{L/R}}$ (set to $\mu=0$ eV in equilibrium). Since we do not focus on the details of the coupling between the molecule and the electrodes, it is sufficiently described by $H_{\mathrm{T,L}}+H_{\mathrm{T,R}}$. The tunneling amplitudes are assumed to be independent of the molecular orbital i and the quantum numbers of the electrode states ν. The coupling strength is then characterized by the parameter $\Gamma^{\mathrm{L,R}} \propto \rho_e |t^{\mathrm{L,R}}|^2$.

Polarons are formed due to strong coupling of electronic and vibrational degrees of freedom. The vibrations labeled α, i are described in H_{vib}, with bosonic operators $B_{\alpha i}$ and $B^\dagger_{\alpha i}$ for the vibrational mode with frequency $\omega_{\alpha i}$, i.e., every part of the molecule can vibrate independently. $H_{\mathrm{el-vib}}$ couples the electrons on the molecule to the vibrational modes, where $\lambda_{\alpha i}$ is the strengths for the local electron-vibration coupling for the site i and mode α, respectively. To ensure energy dissipation and thermal occupation of the vibrational states, we couple every vibration to its own bath $H_{i,\mathrm{bath}}$, the microscopic details of which do not matter.

A perturbative treatment of the strong electron-vibration coupling in the above Hamiltonian is not reasonable. Nevertheless, to allow for a perturbation expansion we apply the so-called polaron or Lang-Firsov unitary transformation,

$$\widetilde{H} = e^S H e^{-S} \qquad (2)$$

with the generator

$$S = -\sum_{\alpha i} \frac{\lambda_{\alpha i}}{\hbar \omega_{\alpha i}} a^\dagger_i a_i [B_{\alpha i} - B^\dagger_{\alpha i}]. \qquad (3)$$

We introduce transformed electron and vibrational operators,

$$\widetilde{a}_i = a_i \chi_i,$$

$$\widetilde{B}_{\alpha i} = B_{\alpha i} - \frac{\lambda_{\alpha i}}{\hbar \omega_{\alpha i}} a^\dagger_i a_i$$

and polaron operators

$$\chi_i = \exp\left[\sum_\alpha \frac{\lambda_{\alpha i}}{\hbar \omega_{\alpha i}}(B_{\alpha i} - B^\dagger_{\alpha i})\right]. \qquad (4)$$

Operators χ_i with different indices i act on different vibrational states, therefore they commute for all times. In terms of these quantities, the Hamiltonian reads

$$\widetilde{H} = \widetilde{H}_0 + \widetilde{H}',$$

$$\widetilde{H}_0 = \sum_i (\epsilon_i - \Delta_i)a^\dagger_i a_i + \sum_{\alpha i} \hbar \omega_{\alpha i}\left(B^\dagger_{\alpha i} B_{\alpha i} + \frac{1}{2}\right) + H_{\mathrm{L}} + H_{\mathrm{R}},$$

$$\widetilde{H}' = -\sum_{\langle ij \rangle} t_{ij} a^\dagger_i \chi^\dagger_i a_j \chi_j + \sum_{\nu,r,i} [t^r c^\dagger_{\nu r} a_i \chi_i + t^{r*} a^\dagger_i \chi^\dagger_i c_{\nu r}], \qquad (5)$$

$$\Delta_i = \sum_\alpha \frac{\lambda^2_{\alpha i}}{\hbar \omega_{\alpha i}}. \qquad (6)$$

$\widetilde{H}'$ describes the perturbation to the exactly solvable Hamiltonian $\widetilde{H}_0$. The perturbation consists of the hopping along the molecule and to/from the electrodes, where the operators χ_i account for the creation and absorption of vibrations in the hopping processes. Without the coupling to vibrations, the perturbation expansion makes sense only if the hopping strengths t_{ij} or t^r are small, e.g., compared to temperature, especially for homogeneous chains. Coupling to vibrations leads to additional factors of the type $\langle \chi^\dagger_i(t) \chi_i(0) \rangle$ (and also expectation values with a larger, even number of χ operator products, cf. Appendix C). These factors are strongly energy-dependent (after Fourier transform) and are known from the so-called "P(E)-theory" of tunneling in a dissipative electromagnetic environment.[17] However, even the peak value of these factors is of order $1/\Delta$, so the perturbation expansion is effectively controlled, if the polaron binding energy Δ is large compared to the hopping strength.

A. Real-time expansion

There are two limits to polaron transport, coherent band-like transport and incoherent hopping transport. For weak electron-vibration coupling and low temperatures coherent transport dominates, whereas for strong coupling and high temperatures transport is a sequence of incoherent hopping processes. In this work, we will focus on incoherent polaron hopping. To describe the physics in this regime, we extend a formalism developed by Böttger and Bryksin[12] for polaron transport in bulk systems to account for coupling to metallic electrodes.

To calculate quantities of interest, e.g. the occupation number $\langle a^\dagger_i(t) a_i(t) \rangle$ and the current in a nonequilibrium situation with applied bias, we make a real-time expansion of the occupation number along the Keldysh contour. The evolution in the interaction picture introduces the time dependence,

$$a_i(t) = a_i e^{-i(\epsilon_i - \Delta_i)t} = a_i e^{-i\widetilde{\epsilon}_i t},$$

$$B_i(t) = B_i e^{-i\omega_i t}.$$

From here on we will use the shifted on-site energy $\widetilde{\epsilon}_i = \epsilon_i - \Delta_i$ in all expressions.

The occupation number of the molecule can be written as $\rho_l(t) = \langle a^\dagger_l(t) a_l(t) \rangle_{\widetilde{H}}$. We express it in the interaction picture, assuming that the perturbation $\widetilde{H}'$ is adiabatically turned on from the time $t_0 = -\infty$,

$$\rho_l(t) = \langle U^\dagger_{\widetilde{H}_0}(t,-\infty) a^\dagger_l a_l U_{\widetilde{H}_0}(t,-\infty) \rangle_{\widetilde{H}_0}$$

with time-evolution operator

$$U_{\widetilde{H}_0}(t,-\infty) = T\left\{\exp\left[-i\int_{-\infty}^t dt \widetilde{H}'_{\widetilde{H}_0}(t)\right]\right\}. \qquad (7)$$

A Taylor expansion of the time-evolution operators in $\widetilde{H}'$ defines a diagrammatic expansion. The forward time-evolution operator $U_{\widetilde{H}_0}(t,-\infty)$ is expanded on the upper branch of the Keldysh contour whereas the backward time-evolution operator $U^\dagger_{\widetilde{H}_0}(t,-\infty)$ is expanded on the lower
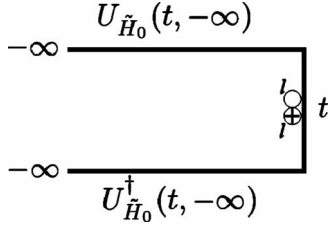
FIG. 2. Schematic drawing of the Keldysh contour and the forward and backward time-evolution operators. The open and crossed circle (the clamp) represent the two operators a_l and $a_l^\dagger$, respectively, which are evaluated at time t.

branch (see Fig. 2). The index $\tilde{H}_0$ indicates that these operators are written in the interaction picture. The time-ordering operator "T" in Eq. (7) (antitime-ordering operator "$\tilde{T}$") ensures that the different times t_i, arising from the Taylor expansion of the forward (backward) time evolution operator, are ordered in the correct way along the contour. Note, oftentimes forward and backward time evolution operators are combined and a contour ordering operator "T_k" is introduced to ensure the correct ordering of times along the Keldysh contour.[18,19]

In performing the expansion in the time-evolution operators, we obtain certain operator products, which we have to average thermally. Since $\tilde{H}_0$ is quadratic in the fermion operators, these can be treated using Wick's theorem. On the other hand, the vibrational operator products, involving various operators $\chi_i(t_j)$, cannot be factorized. The rules for the evaluation of these operator products are given in Appendix C.

A specific term in the Taylor expansion, is represented by a diagram with a certain number of vertices on the upper and lower branch of the Keldysh contour, where each vertex is proportional either to t_{ij} (a hopping vertex) or t^r (a tunneling vertex). Each vertex consists of one open circle ○ (symbolizing a destruction operator) and one crossed circle ⊕ (symbolizing a creation operator). All circles belonging to operators acting on the molecule are drawn on the inside of the contour whereas circles belonging to electrode operators are drawn on the outside of the contour (compare, e.g., Fig. 3).
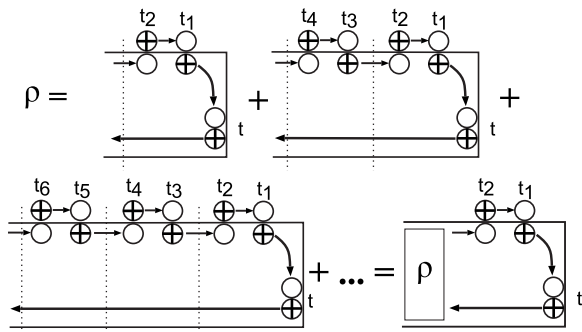

FIG. 3. Ladder summation of a second-order irreducible block representing two tunneling processes. The irreducible blocks are separated by free sections (indicated by dotted lines). The summation can be recast into a self-consistency equation for the occupation number ρ.
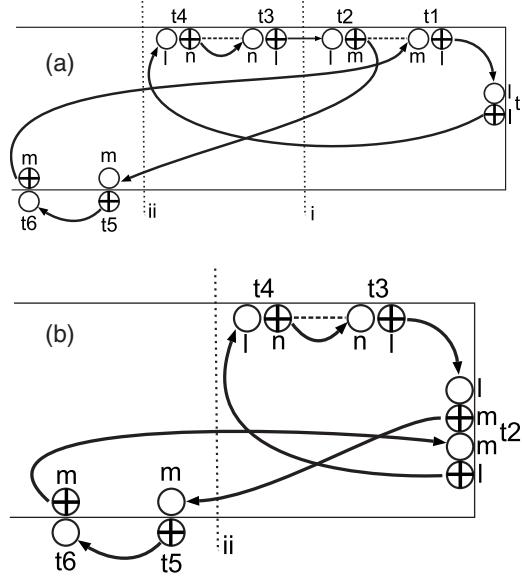

FIG. 4. (a) Sixth-order diagram in the real-time expansion of the occupation number $\langle U_{\tilde{H}_0}^\dagger(t) a_l^\dagger a_l U_{\tilde{H}_0}(t) \rangle$ (b) Fourth-order diagram in the real-time expansion of the two-particle correlation function $\langle U_{\tilde{H}_0}^\dagger(t_2) a_l^\dagger a_m a_m^\dagger a_l U_{\tilde{H}_0}(t_2) \rangle$. Free sections are indicated by the vertical dotted lines.

The different vertices are connected by fermion (solid) and vibrational (dashed) lines and belong to different times t_i, which have to be (anti) time ordered along the (lower) upper branch of the contour.

A feature of this expansion is that certain diagrams are diverging even in first order. These diagrams can be identified by so called "free sections" (indicated by the dotted lines in Fig. 3). A free section is a part of the diagram between two vertices (except for the clamp) where a vertical line can be drawn such that only internal fermion lines are cut (neither a phonon line nor an external fermion line belonging to the electrodes). In such a case, the vertical line always cuts an even number of internal fermion lines, as many left as right going. These left- and right-going lines are pairwise associated with the same site. In the evaluation of such a diagram, this leads to a divergence which arises from the integral $\int_{-\infty}^t dt' \exp[-i(\tilde{\epsilon}_m - \tilde{\epsilon}_l)t']$ with $l = m$. Physically this corresponds to a free propagation for an infinitely long time. Thus, an infinite number of diagrams has to be summed up in a way similar to a "ladder" approximation.[12,20,21] The regions in between free sections (excluding the clamp) are called irreducible blocks. They do not diverge.

In Fig. 3 such a ladder summation of a second-order irreducible block representing a tunneling process is shown. Similar to a Dyson series, the summation of an infinite number of diagrams can be written as a self-consistent equation for the occupation number ρ.

For the interacting system we consider, certain diagrams lead to equations coupling the occupation number to many-particle correlation functions. This is illustrated in Fig. 4. The dotted vertical lines denoted (i) and (ii) indicate free sections which lead to divergences. Let us concentrate on the free section (i) in Fig. 4(a). To cure the divergence due to (i),
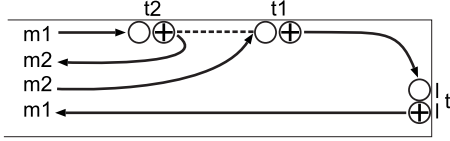
FIG. 5. A second-order hopping diagram. The full lines represent fermion lines. The dashed line represents the sum of all possible vibrational lines arising from the diagrammatic rules, here it has a value $F_l^+(t_1-t_2)F_{m_2}^+(t_1-t_2)+F_l^+(t_1-t_2)+F_{m_2}^+(t_1-t_2)$ [cf. Appendix A].

a ladder summation has to be performed over all diagrams with the same divergence, i.e., the same free section. This can be done in a complete and tractable manner by the introduction of many-particle correlation functions.

Aside of this technical argument, there are also simple physical arguments why (and when) the two-particle correlation functions affect the behavior of the occupation numbers (and the current). Consider a hopping process from sites m to site n: the hopping probability is determined by a second-order irreducible diagram and the occupation of the initial and final site. Two-particle correlation functions express the probability to find, e.g., the initial site m occupied and the final site n empty, such that the hopping process can succeed. In general, the occupation of different sites is correlated, except in the trivial case when there is exactly one particle on the (central) system. If the charge density is finite, but very low, the charges are well described by a Boltzmann distribution[22,23] and the two-particle correlation functions can be factorized in a "Hartree-Fock" type of approximation. This approach was taken in earlier works.[11,21–23]

B. A hierarchy of many-particle correlation functions

By inspection of the part of diagram Fig. 4(a) *left* of the free section (i) one notices that this resembles a diagram arising from the real-time expansion of the two-particle correlation function $\langle U_{\tilde{H}_0}^\dagger(t_2)a_l^\dagger a_m a_m^\dagger a_l U_{\tilde{H}_0}(t_2)\rangle$, see Fig. 4(b). Straightforward generalization shows that the ladder summation for the diagram 4(a) consists of all diagrams that arise from the real-time expansion of this particular two-particle correlation function, placed to the left of the free section (i), as indicated by Fig. 5. In this way, an infinite number of diagrams to the occupation number ρ can be accounted for by involving this particular two-particle correlation function with the particular irreducible block, given by the right part of the diagram in Fig. 4(a) from the free section indicated by (i) to the last vertex before the clamp. Other irreducible blocks involve other type of many-particle correlations functions. What kind of correlation function is needed can be read off from the vertices of the irreducible block (following the contour) that are connected to the fermion lines crossing the free section (see also Appendix B).

Figure 4(b) is only a particular diagram to the expansion of the two-particle correlation function $\langle U_{\tilde{H}_0}^\dagger(t_2)a_l^\dagger a_m a_m^\dagger a_l U_{\tilde{H}_0}(t_2)\rangle$. However, the arguments for replacing the free section (ii) in this diagram work the same way as for the expansion for the occupation number ρ.
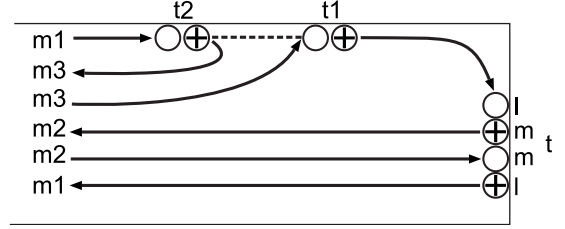

FIG. 6. A second-order hopping diagram. The full lines represent fermions, the dashed line represents the sum of all possible vibrational lines arising from the diagrammatic rules, here it has a value $F_m^+(t_1-t_2)F_{m_3}^+(t_1-t_2)+F_m^+(t_1-t_2)+F_{m_3}^+(t_1-t_2)$.

Therefore, we can write a linear equation for this two-particle correlation function involving all other two-particle correlation functions, the occupation number ρ and other many-particle correlations functions. These many-particle correlations fulfill yet another set of linear equations.

In this manner, a hierarchy of linear equations is established. In principle, the approximation to the exact solution of the problem lies so far solely in the limited number of irreducible blocks that can be considered in a real calculation, i.e., in the order of expansion of the irreducible blocks in the hopping and tunneling vertices. In practice, the question arises whether the hierarchy of equations can be solved exactly, or whether other approximations need to be applied, like a truncation or a factorization of the many-particle correlations functions.

C. Truncation of the hierarchy

An important feature of the real-time expansion of the correlation functions is that certain diagrams vanish due to the Pauli exclusion principle. For example, the diagram depicted in Fig. 6 arises in the expansion of the two-particle correlation function and describes hopping process from site $m\equiv m_2$ to m_3 at time t_2 and back to m at time t_1. To its left the irreducible block is coupled to the three-particle correlation function $\langle U_{\tilde{H}_0}^\dagger(0)a_{m_1}^\dagger a_{m_1} a_{m_2}^\dagger a_{m_3} a_{m_3}^\dagger a_{m_2} U_{\tilde{H}_0}(0)\rangle$ with $m_1 \equiv l$. For $m_3=m_1\equiv l$ there arises a special situation, the three particle correlation function is zero since for fermions $\hat{n}_l(1-\hat{n}_l)=0$ with $\hat{n}_l=a_l^\dagger a_l$.

Furthermore, by similar arguments the Pauli exclusion principle leads to a *natural truncation* of the hierarchy of equations for *any finite* system. The N-particle correlation function $\langle U_{\tilde{H}_0}^\dagger(0)a_1^\dagger a_1 a_2^\dagger a_2\cdots a_N^\dagger a_N U_{\tilde{H}_0}(0)\rangle$ cannot couple to any higher-order correlation function because they all vanish (recall that N is the system size.) Thus, a closed set of *linear* equations for the real-time expansion of all correlation functions can be constructed. The formal solution of this set of equations is simply a matter of backsubstitution.

In the earlier works,[11,21–23] a Hartree-Fock factorization was applied in which products of particle number operators are replaced their expectation values. This leads to terms in the expansion that should not exist if the exact correlation functions were considered. The differences to the full theory are small, if the electron or hole densities are so low that they can be described by Boltzmann statistics. However, there is

the additional complication that the factorization leads to a *nonlinear* self-consistency equation for the occupation numbers ρ_i. At finite bias it can be quite difficult to find a converging solution, especially as the system size becomes larger. This difficulty is avoided in our present theory where a solution to the linear equation set can be readily found by standard numerical methods. Note, however, that the number of correlation functions grows exponentially ($\sim 2^N$ for spinless fermions), so our method is limited to short chains. For long chains, a truncation of the hierarchy at some level (beyond Hartree-Fock) is still needed. For the system we considered, factorizations of correlation function of the three-particle level (and higher) proved to be very close to the exact solution of the hierarchy (provided the nonlinear equations converged).

Summarizing the above, the relation

$$\frac{d}{dt}\rho_l(t) = \int_{-\infty}^{t} dt_1 \bigg[\sum_{m_1} \varrho_{m_1}(t_1)\mathcal{W}_{m_1 l}(t_1 - t) + \sum_{m_1 m_2} \varrho_{m_1 m_2}(t_1)\mathcal{W}_{m_1 m_2 l}(t_1 - t) + \dots \bigg] \quad (8)$$

for the time derivative of the occupation number is obtained. The diagrammatic rules for construction and evaluation of irreducible blocks $\mathcal{W}$ are listed in Appendix A. The generalized (one- and two-particle) correlation functions ϱ_{m_1} ($\varrho_{m_1 m_2}$) represent any order of the creation and destruction operators a_{m_1}, $a_{m_1}^{\dagger}$ ($a_{m_1}, a_{m_1}^{\dagger}, a_{m_2}, a_{m_2}^{\dagger}$) that arises in the free sections. Using the commutation relations for fermions, all generalized correlation functions $\varrho_{m_1 \dots m_j}$ can be expressed by a sum of correlation functions $\rho_{m_1 \dots m_i}$ (of the same or lower order) where we fix the order of creation and destruction operators such that the creation operators at a site are to the left of there destruction counterparts, i.e., $\rho_{m_1 \dots m_i} \equiv a_{m_1}^{\dagger} a_{m_1} \dots a_{m_i}^{\dagger} a_{m_i}$. In the rest of this paper, we only use these ordered correlation functions $\rho_{m_1 \dots m_i}$ (note that the occupation number is naturally defined by the one-particle correlation function ρ_{m_1}).

D. Explicit equations for the considered model

In this paper, we want to calculate the stationary state of the system when a constant, finite bias is applied between the metallic electrodes. Therefore, all correlation functions must be constant in time as well, such that Eq. (8) reduces to

$$0 = \frac{d}{dt}\rho_l = \sum_{m_1} \varrho_{m_1} \int_{-\infty}^{t} dt_1 \mathcal{W}_{m_1 l}(t_1) + \sum_{m_1 m_2} \varrho_{m_1 m_2} \int_{-\infty}^{t} dt_1 \mathcal{W}_{m_1 m_2 l}(t_1) + \dots . \quad (9)$$

Furthermore, we restrict ourselves to the lowest nonvanishing order of diagrams, i.e., second order. Examples of two such diagrams in the expansion of the occupation number and two-particle correlation functions are given in Figs. 5 and 6. When comparing these two diagrams, it is clear that they are mostly identical except for two additional fermion lines in Fig. 6 which enter as Kronecker-delta symbol. Of

course, the corresponding irreducible blocks $\mathcal{W}$ couple to different correlation functions determined by the fermion lines leaving to and entering from the left.

According to the "mirror" rule, to every diagram one can construct its complex conjugate by moving a vertex from the upper part of the contour to the lower one (and vice versa). Following the rules given in the appendix the two diagrams (Figs. 5 and 6) together with their respective complex conjugates and including the time integral of Eq. (9) have the values

$$\mathcal{W}_{m_1 m_2 l} = -\frac{|t_{l,m_2}|^2}{\hbar^2} \mathcal{K}_l^2 \mathcal{K}_{m_2}^2 \int dt \, e^{i/\hbar(\bar{\epsilon}_l - \bar{\epsilon}_{m_2})t} \times [F_l^+(t)F_{m_2}^+(t) + F_l^+(t) + F_{m_2}^+(t)]\delta_{lm_1} \quad (10)$$

and

$$\mathcal{W}_{m_1 m_2 m_3 lm} = -\frac{|t_{m,m_3}|^2}{\hbar^2} \mathcal{K}_m^2 \mathcal{K}_{m_3}^2 \int dt \, e^{i/\hbar(\bar{\epsilon}_m - \bar{\epsilon}_{m_3})t} \times [F_m^+(t)F_{m_3}^+(t) + F_m^+(t) + F_{m_3}^+(t)]\delta_{lm_1}\delta_{mm_2}. \quad (11)$$

Explicit expressions for the constants $\mathcal{K}_l$ and the functions $F_l^+(t)$ are given in the Appendix A. The common element of all second-order hopping diagrams in the expansion of the various correlation functions may be defined as

$$\mathcal{W}_{lm} = \frac{|t_{l,m}|^2}{\hbar^2} \mathcal{K}_l^2 \mathcal{K}_m^2 \int dt \, e^{i/\hbar(\bar{\epsilon}_l - \bar{\epsilon}_m)t} \times [F_l^+(t)F_m^+(t) + F_l^+(t) + F_m^+(t)]. \quad (12)$$

For the second-order diagrams describing the hopping to and from the electrodes there exist also such common elements. They are, respectively,

$$W_-^L = \Gamma^L \int \frac{dE}{2\pi\hbar}(1 - f_L(E))\mathcal{K}_1^2(F_1^+(\bar{\epsilon}_1 - E) + \delta(\bar{\epsilon}_1 - E)),$$

$$W_+^L = \Gamma^L \int \frac{dE}{2\pi\hbar}f_L(E)\mathcal{K}_1^2(F_1^+(E - \bar{\epsilon}_1) + \delta(E - \bar{\epsilon}_1)), \quad (13)$$

where $\Gamma^L = 2\pi|t^L|^2\rho_e$, $f_L(E)$ is the Fermi function in left lead, and $F_1^+(E)$ is the Fourier transform of $F_1^+(t)$. For the right interface a similar expression holds involving $f_R(E)$ and $F_N^+(E)$.

Evaluating all second-order diagrams simplified rate equations for the single-particle occupation number can be stated as

$$\frac{d}{dt}\rho_l = \sum_m \left[-(\rho_l - \rho_{lm})\mathcal{W}_{lm} + (\rho_m - \rho_{ml})\mathcal{W}_{ml} \right], \quad (14)$$

$$\frac{d}{dt}\rho_1 = -\rho_1 W_-^L + (1-\rho_1)W_+^L - (\rho_1 - \rho_{12})\mathcal{W}_{12} + (\rho_2 - \rho_{21})\mathcal{W}_{21}.$$

(15)

For the two-particle correlation functions on the inside of the molecule and connected to the left electrode the rate equations have similar form

$$\frac{d}{dt}\rho_{lm} = \sum_n \left[-(\rho_{lm} - \rho_{lmn})\mathcal{W}_{ln} + (\rho_{mn} - \rho_{lmn})\mathcal{W}_{nl} \right.$$
$$\left. -(\rho_{lm} - \rho_{lmn})\mathcal{W}_{mn} + (\rho_{ln} - \rho_{lmn})\mathcal{W}_{nm} \right]$$

(16)

and

$$\frac{d}{dt}\rho_{12} = -\rho_{12}W_-^L + (\rho_2 - \rho_{12})W_+^L$$
$$-(\rho_{12} - \rho_{123})\mathcal{W}_{23} + (\rho_{13} - \rho_{123})\mathcal{W}_{32}.$$

(17)

All other rate equations not presented above are constructed in an analogous way. This leads to a closed set of linear equations for all correlation functions up to the order of the system size N.

The theory is current conserving as Eqs. (14) and (15) are the continuity equations for the occupation of site l and 1, respectively, which equal zero in the steady-state situation we consider. Thus the current can be computed at any point of the entire system. For convenience, we choose to compute the current through the left lead given by

$$I_L = e[-\rho_1 W_-^L + (1-\rho_1)W_+^L].$$

(18)

Note that all many-particle correlation functions drop out of this expression. They influence the current only via their effect on the occupation at the first site, ρ_1.

E. Polaron hopping transport in DNA

In this section, we apply the above presented diagrammatic approach to polaron hopping transport in DNA, which we have already studied earlier in a more simplified approach, involving the Hartree-Fock factorization.[11] DNA consists of a sequence of base pairs adenine and thymine and guanine and cytosine, which form a double helical ladder structure. The electronic properties of DNA are determined by the HOMO, situated on the guanine and adenine bases, and the LUMO, situated on cytosine and thymine bases.[24]

To describe polaron-hole hopping, the relevant molecular orbital is the HOMO. We describe the DNA chain in a minimal tight-binding model where each tight-binding site represents one HOMO either on a guanine or an adenine base. Both on-site energies ϵ_i and hopping integrals t_{ij} depend on the base pair sequence. For the direction-dependent hopping matrix elements t_{ij} we use the values obtained from density functional theory by Siebbeles et al.[25] Adapting these values to our model of base pairs we obtain the next-neighbor hopping elements listed in Table I.

As shown by Alexandre et al.[26] and also other authors[27–29] polarons are formed on DNA molecules, although the size of these polarons is still controversial. Fits to the temperature dependence of the linear conductance of experiments on long

($>$1000 base pairs) DNA segments like Ref. 1 support the idea of small polaron formation with a local DNA distortion.[30,31] In this work, we assume that the size of polarons is restricted to single DNA base pairs. Such small polarons are formed due to strong coupling of the electronic degrees of freedom to local vibrational modes of the DNA base pairs. Exemplary, we consider only a single vibrational mode per base-pair, the so-called stretch modes with frequencies $\hbar\omega_i = 16$ meV for a GC base pair and $\hbar\omega_i = 11$ meV for an AT base pair.[32]

The electron-vibration coupling strengths are chosen in such a way that the reorganization energy or polaron shifts [compare Eq. (6)], $\nu_A = 0.18$ eV and $\nu_G = 0.47$ eV, fit the values extracted from experiments and listed by Olofsson et al.[33] These values probably underestimate the effect of the solvent on the reorganization energy.

To ensure energy dissipation and thermal occupation of the vibrations each base pair i is coupled to a local environment, $H_{i,\text{bath}}$, the microscopic details of which do not matter. This coupling changes the vibrations' spectra from discrete modes ω_i to continuous spectra,

$$D_i(\omega) = \frac{1}{\pi}\left(\frac{\eta_i(\omega)}{(\omega - \omega_i)^2 + \eta_i(\omega)^2} - \frac{\eta_i(\omega)}{(\omega + \omega_i)^2 + \eta_i(\omega)^2} \right)$$

(19)

with frequency dependent broadening $\eta_i(\omega)$.[6] The actual form of $\eta_i(\omega)$ depends on the properties of the bath. A reasonable choice which assures also convergence at low and high frequencies is $\eta_i(\omega) = \eta_0 \frac{\omega^3}{\omega_i^3}\theta(\omega_c - \omega)$ with $\eta_0 = 0.5$ meV and a cutoff of the order of $\hbar\omega_c = 0.045$ eV. To account for the spectral function of the base pair vibrations, the substitution $\Sigma_\alpha \rightarrow \int d\omega D_i(\omega)$ has to be made in all equations introduced above.

III. RESULTS

The main focus of this paper is the investigation of the influence of correlations on the electronic transport characteristics. To do so, we compare our present theory with exact correlation effects to our previous approach involving a Hartree-Fock factorization that deals with correlations only on the mean-field level. For simplicity, we denote the latter approach as "mean-field correlations."

It should be noted that correlation effects do not influence the transport properties of homogeneous DNA sequences or other homogeneous molecules. This is because for a homogeneous system, not only $\rho_{lm} = \rho_{ml}$ (this is always true by definition of the correlation functions), but also the hopping rates for forward and backward hopping processes are identical, $\mathcal{W}_{lm} = \mathcal{W}_{ml}$. Therefore, the two-particle correlation functions drop out of Eqs. (14) and (15) for the occupation numbers, and consequently do not influence the current. The I-V curves are therefore identical, no matter whether exact correlations or mean-field correlations are considered.

A. Zero-bias conductance

As noted earlier the difference between the two approaches is small, when the occupation of holes or electrons
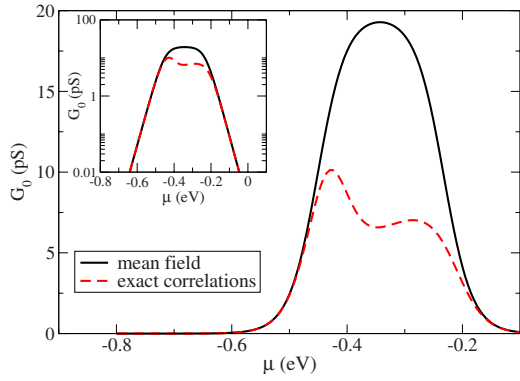
FIG. 7. (Color online) Zero-bias conductance G_0 as a function of chemical potential μ for the DNA molecule with sequence AAAGAAAA with mean-field correlations (black solid line) and exact correlations (red dashed line). The parameters used are $\epsilon_A = -0.26$ eV, $\epsilon_G = +0.25$ eV relative to the zero point of the chemical potential, polaron shifts $\Delta_A = 0.18$ eV and $\Delta_G = 0.47$ eV, symmetric coupling to leads with linewidths $\Gamma_L = \Gamma_R = 0.001$ eV, vibrational energies $\hbar\omega_A = 11$ meV, $\hbar\omega_G = 16$ meV, and room temperature $k_B T = 25$ meV. The inset shows the same plot on logarithmic scale to stress that both models agree for very low and high occupation.

is small so that the occupation is described by a Boltzmann distribution function. To demonstrate this Fig. 7 shows the zero-bias conductance G_0 as a function of chemical potential μ of the equilibrium electrodes for a DNA molecule with sequence AAAGAAAA with mean-field correlations (black solid line) and exact correlations (red dashed line). We have chosen the reference point $\mu = 0$ to lie above the (polaron shifted) guanine and adenine states, i.e., in the HOMO-LUMO gap of DNA. As can be seen from the figure, especially from the inset on logarithmic scale, for values of $\mu < -0.5$ eV and above $\mu > -0.15$ eV the two curves agree with each other. In the first region, the electron occupation number is very small, whereas in the latter the hole occupation is very low. On the other hand, in the central region of the plot both curves differ strongly. The zero-bias conductance is much lower when correlation effects are exactly accounted for. Furthermore, the red curve exhibits two maxima around the chemical potentials that agree with the on-site energies of adenine ($\tilde{\epsilon}_A$) and guanine ($\tilde{\epsilon}_G$). The black curve, with mean-field correlation effects, only shows a single broad maximum. Similar to coherent quantum transport through molecules, the mean-field type approximation of correlations overestimates the (zero-bias) conductance and current and only shows a very simplified energetical structure.

As an illustration, the effect of exact correlations on the occupation of the bases for the sequence AAAGAAAA is shown in Fig. 8. The curves show the difference of the occupation for the two approaches for the first (black solid line) fourth (red dashed line) and eighth (blue dashed-dotted line) base of the DNA molecule AAAGAAAA as a function of chemical potential μ. The values were calculated for a small transport bias $V_b = 0.01$ V, which is in the linear regime. The sign and magnitude of the occupation difference changes with the bias direction and strength, respectively.
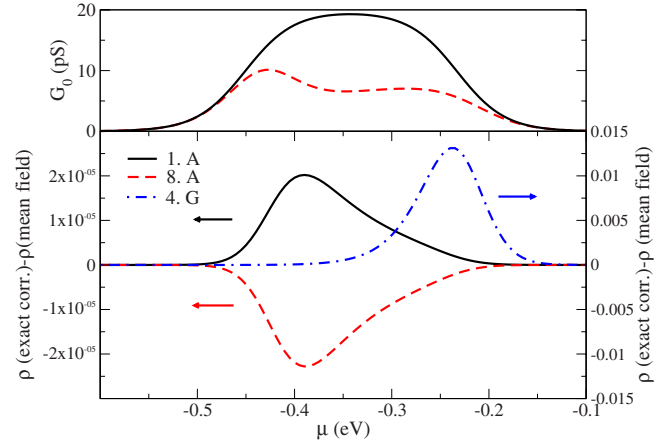
FIG. 8. (Color online) Lower graph: difference of the occupation for exact and mean-field correlations for the first (black solid line) fourth (red dashed line) and eighth (blue dashed-dotted line) base of the DNA molecule AAAGAAAA as a function of chemical potential μ. The used transport bias is $V_b = 0.01$ V, which is in the linear regime. As reference in the upper graph the plot of Fig. 7 is repeated. Parameters as in Fig. 7.

The maximum in occupation difference for the adenine and guanine bases is reached for chemical potential values which are close to the on-site energies of either adenine or guanine, respectively. The effect of the correlation is the strongest for the isolated guanine base in the center of the sequence, where the maximum difference in occupation is three orders of magnitude greater than for the adenine bases. The occupations of the other adenine bases (not shown), are similar to the ones depicted in Fig. 8.

B. Finite-bias differential conductance

In experiments, a variation in the chemical potential is rather difficult to achieve. In molecular electronics, this is usually achieved by using a backgate electrode under an insulating substrate. However, for DNA the complication arises that its conformational structure is much influenced by the surface potential of the substrate and the electric potentials of the back gate. Oftentimes, though, the I-V characteristics can be probed in setups where the molecules are in free suspension (mechanical break junctions) or standing upright in molecular monolayers.

When applying a transport bias $V_b = \mu_L - \mu_R$ over the molecule, rather than applying a linear profile we let the external potential drop at the two electrode-molecule interfaces by equal amounts. For the applied bias range considered, the difference is minor for inhomogeneous chains. Homogeneous chains are slightly more disturbed as they become in effect also inhomogeneous so correlation effects will be present to a small degree. We neglect image charge effects. They could be relevant, if the sequence differs from homogeneity only at the contact base pair.

At finite transport bias, the occupation of the various molecular segments (base pairs in the case of the DNA) changes from their equilibrium values. These occupational changes can be translated into local potentials. The resulting potential
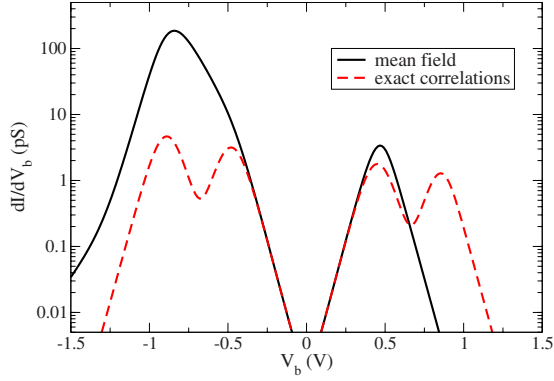
FIG. 9. (Color online) Differential conductance dI/dV_b (logarithmic scale) as a function of applied bias V_b for the DNA molecule with sequence AAAGAAAA, for mean-field correlations (black solid line) and exact correlations (red dashed line). Parameters as in Fig. 7 but with the equilibrium chemical potential of the electrodes fixed at $\mu = 0$ eV.

FIG. 10. (Color online) The zero-bias conductance G_0 as a function of chemical potential μ for the DNA sequence AAAGGAAA (black solid line) with exact correlations. Only a single maximum around the guanine energy is displayed. For the dashed line the hopping rate between the two central guanine bases is enhanced by a factor 100. This shows that the maximum at the adenine energy in the sequence AAAGGAAA is suppressed due to the peculiar hopping parameters relevant for DNA. Other parameters as in Fig. 7.

profile can be interpreted as a position dependent "local chemical potential" that changes with the applied bias. As this local chemical potential moves over the energies of the base pair levels, similar effects as in Fig. 7 are expected. In Fig. 9 we show the differential conductance dI/dV_b as a function of applied transport bias V_b. The red curve including exact correlation effects shows two maxima for both positive and negative bias whereas the black line with mean-field correlations only has single peaks. For small bias both curves agree very well, as the charge carrier occupation in this regime is very low. Note that again the mean-field approach overestimates the (differential) conductance everywhere, except for large positive bias, where the second peak exists in a bias region where the mean-field approach shows exponentially small conductance.

From these calculations it becomes clear that at finite transport bias the charge carrier occupations have regions, where mean-field type of correlations are insufficient to describe polaron hopping transport through molecules like DNA.

We now discuss the position of the maxima in the zero-bias and differential conductance. For a homogeneous molecule, both G_0 and dI/dV_b only have a single maximum, namely when the chemical potential (or the transport bias) is in resonance with the level energy of the DNA base pairs ($\tilde{\epsilon}_G = -0.22$ eV and $\tilde{\epsilon}_A = -0.44$ eV). Including exact correlations, for the DNA molecule AAAGAAAA there are two maxima in the zero-bias conductance as a function of chemical potential, or in the differential conductance, for both positive and negative transport bias (see Figs. 7 and 9). These maxima can also be associated with the level energies of the two different types of bases, adenine and guanine. However, the exact positions of the maxima in the zero-bias conductance deviate slightly from their expected resonance positions due to charge rearrangement effects between guanine and adenine bases. Since the hopping rates increase strongly with temperature, the charge rearrangement also increases. Thus the position of the maxima is temperature dependent.

For the differential conductance, the positions of the maxima are shifted more strongly as a finite transport bias

will lead to much stronger charge rearrangements (polarization). This effect is increasingly important for the maxima at higher bias, i.e., the second maxima are shifted more strongly from the anticipated resonance positions of the adenine bases energy as compared to the first maxima relating to the guanine energies. The charge rearrangement and therefore the position of the conductance maxima is quite sensitive to the considered DNA sequence (see also discussion in Ref. 11).

C. Sequence effects

Are there always as many maxima as different species of molecular segments with different on-site energies, if exact correlations are considered? The black solid curve in Fig. 10 shows the zero-bias conductance as a function of chemical potential for the DNA sequence AAAGGAAA. This sequence is only a slight modification as compared to AAAGAAAA studied above, nevertheless the zero-bias conductance exhibits only a single maximum, the "adenine"-peak is missing. A similar behavior is observed for the differential conductance as a function of applied bias.

Does this mean that for this sequence the adenine resonance does not occur? It turns out that it is just suppressed. The red dashed curve in Fig. 10 is calculated for the same sequence but with a hopping rate $\mathcal{W}_{GG}$ enhanced by a factor 100. In this curve again two maxima are visible, both in the zero-bias and differential conductance. Obviously, the adenine resonances were present but the resulting transport is strongly suppressed by the low hopping rate $\mathcal{W}_{GG}$ for our model of DNA parameters.

At first glance, it might appear strange that the hopping rate between two guanine base pairs is so much limiting the transport at energies related to the adenine base pairs. However, this effect can be easily explained by looking at the current between the two guanine bases of the above DNA sequence. From Eq. (14) one can deduce

$$I = e(\rho_4 - \rho_{45})\mathcal{W}_{45} + e(\rho_5 - \rho_{45})\mathcal{W}_{54} = e(\rho_4 - \rho_5)\mathcal{W}_{GG}, \tag{20}$$

where the sites 4 and 5 denote the two guanine bases and for the second line $\mathcal{W}_{45} = \mathcal{W}_{54} = \mathcal{W}_{GG}$ was used.

As the current is conserved, the above equation is identical to the current obtained from Eq. (18). Obviously, a small rate $\mathcal{W}_{GG}$ leads in general to a small current. However, the important matter lies in the difference of occupations $(\rho_4 - \rho_5)$ of the two guanine bases (for a small applied transport bias) that varies strongly depending on the chemical potential. For the DNA sequence AAAGGAAA, the current reaches its maximum value when the difference in occupation between the two guanine sites is the greatest. This is the case when the guanine on-site energy is in resonance with the chemical potential, i.e., around $\mu = -0.22$ eV, as at this energy the guanine occupation changes rapidly from unity to zero while lowering the chemical potential. For much lower values of the chemical potential (in particular, $\mu \approx -0.44$ eV) the occupation of the guanine bases is already close to zero and thus the occupation *differences* are also small. The double guanine segment limits the current the molecule can support at the adenine energy around -0.44 eV.

If we artificially enhance the rate $\mathcal{W}_{GG}$ by a factor 100, see dashed line in Fig. 10 the conductance is overall increased, though not by a factor of 100. The increase is much stronger around the adenine energy than around the guanine energy. Removing the original bottleneck, even small occupation differences between the guanines lead now to a fairly sized conductance around the adenine energy. As the conductance at the guanine energy increases only slightly *despite* the 100-fold increased rate, the guanine occupation difference at the guanine energy is actually *reduced* almost by the same factor. Similar argument hold again for the suppression of the adenine related maxima in the differential conductance.

IV. SUMMARY

We have presented a diagrammatic real-time approach to polaron hopping through molecules coupled to metallic electrodes, taking into account vibration-mediated charge correlations. This technique leads to a hierarchy of linear rate equations for the occupation and many-particle correlation functions, which is naturally truncated for a finite-size system. Thus, an exact description of correlation effects is possible for a given order of the perturbation expansion in the hopping parameters. Using short DNA molecules as an example, we show that including exact correlations lowers the zero-bias conductance of inhomogeneous DNA sequences when the average charge occupation is sufficiently high. For exponentially small charge occupation, a mean-field description of the correlations is adequate. For the *I-V* characteristics, the inclusion of exact correlation effects is necessary since at the experimentally relevant bias voltage the local charge densities are generally non-negligible. We further have shown that for short DNA molecules consisting of two different types of base pairs, the zero-bias and differential conductance shows two maxima. Depending on the specific sequence, one of these maxima can be suppressed due to low hopping rates.

APPENDIX A: CONSTRUCTION OF IRREDUCIBLE BLOCK DIAGRAMS

Below we will state the rules for the construction and evaluation of irreducible block diagrams. The rules for pure hopping diagrams, i.e., those containing only vertices $\propto t_{ij}$, were developed by Böttger and Bryksin.[12] We extended their theory adding new rules to treat diagrams with tunneling vertices $\propto t_{iv}^r$.

The perturbative expansion can be visualized by the construction of diagrams which are equivalent to expressions in the analytic expansion. The main contribution to the diagrams comes from so-called irreducible blocks, which, as the name implies, cannot be decomposed into more simple diagrams. The main feature of an irreducible block diagram is, that it does not diverge, when integrating over the internal times t_i. Irreducible blocks can be identified by their property of not allowing free sections. A free section is a vertical line drawn between the leftmost vertex and the rightmost vertex (except for the clamp) that does not cross either a phonon line or an external fermion (tunneling) line.

The rules come in two sets: the first for the construction and labeling of possible diagram, the second set for the evaluation of a particular diagram. The rules are general for all orders of perturbation theory.

(1) Draw the Keldysh time contour as a rectangle which is open to the left, corresponding to $t \to -\infty$.

(2) For a diagram of order n we draw on the contour $n+1$ pair vertices consisting of one open circle $\bigcirc$ (symbolizing a destruction operator) and one crossed circle $\oplus$ (symbolizing a creation operator). All circles belonging to operators acting on the molecule are drawn on the inside of the contour whereas circles belonging to electrode operators are drawn on the outside of the contour. Therefore, if the pair vertex is due to a tunneling process t^r one circle is on the inside and the other one is on the outside of the contour. The circles of a hopping process are both drawn on the inside of the contour where the open circle is always "earlier" along the Keldysh contour than the crossed circle. As we calculate diagrams to evaluate the density matrix, we draw one pair vertex (also called "clamp"[12]) at the inside of the right vertical line of the Keldysh contour, corresponding to time t. The other n vertices are drawn at n times t_i on either the upper or lower branch of the Keldysh contour (where t_2 is the leftmost, earliest time and t_1 is the rightmost, latest time).

(3) Each open circles $\bigcirc$ on the inside of the contour has one ingoing fermion line (arrow pointing to the vertex) and each crossed circle $\oplus$ has one outgoing fermion line (arrow pointing away from the vertex) which is locally directed along the Keldysh contour.

(4) Complementary circles outside the contour are pairwise connected by a fermion line drawn *outside* of the contour. Since this line corresponds to an electron propagating in electrode r the connected circles have to belong to the same electrode r, otherwise the diagram contribution is zero.

(5) The clamp is always connected by a fermion line to the rightmost vertex (other than the clamp) drawn *inside* of the contour, i.e., the clamp and the rightmost vertex are associated with the same state. If the rightmost vertex is a hopping vertex, the fermion line is directed along the contour. If the rightmost vertex is a tunneling vertex, the inside circle (open or crossed) is connected to the complementary circle of the clamp, no matter what the direction of the fermion line.

(6) The remaining unconnected inside circles have fermion lines going into (coming from) the region left of the diagram ($t \rightarrow -\infty$) without intersecting each other.

(7) Each circle belongs to one specific state for the molecule or the electrode. We label the molecule states (sites) by latin characters (e.g., $m, n, \dots$) and the electrode states by Greek characters (e.g., ν). Note that the two circles of a hopping vertex cannot correspond to the same state (site). Since we want to calculate the density matrix ρ_l then both circles of the clamp are associated with the state (site) l.

(8) Except for the clamp, the circles on the inside of the contour must be connected by phonon lines so that the diagram has no free section, as defined above. One circle can be connected to more than one phonon line. All diagrams with different number of phonon lines (but still without free sections) have to be considered. Only circles belonging to the same state (site) can be connected by a phonon line. Therefore, the two circles of a hopping vertex cannot be connected.

The rules for evaluating a diagram are as follows:

(1) A hopping vertex at time t_i is associated with a factor $\pm i t_{nm} \mathcal{K}_n \mathcal{K}_m e^{-i(\epsilon_n - \epsilon_m)(t_i - t_2)}$ where the creation operator (crossed circle) corresponds to site label n and the destruction operator to the site label m (recall that t_2 is the leftmost time of the diagram). A tunneling vertex is associated with a factor $\pm i t^r \mathcal{K}_m e^{-i(\epsilon_\nu - \epsilon_m)(t_i - t_2)}$ or $\pm i t^r \mathcal{K}_n e^{-i(\epsilon_n - \epsilon_\nu)(t_i - t_2)}$ if the creation operator acts on the electrode or on the molecule, respectively. Vertices on the upper half of the contour have the minus sign, vertices on the lower half of the contour have the plus sign. The factor

$$\mathcal{K}_m = \exp\left\{ -\frac{1}{2} \sum_\alpha \left(\frac{\lambda_{\alpha m}}{\omega_\alpha} \right)^2 (2N(\omega_\alpha) + 1) \right\}.$$

(2) The outside fermion lines of the electrodes r contribute a factor $1 - f_\nu^r$ or f_ν^r depending whether they run in the direction of the contour or against it. Here f_ν^r is the Fermi function at energy $\epsilon_\nu - \mu_r$, with the chemical potential μ_r.

(3) The fermion lines entering (leaving) the irreducible block from (to) the left are labeled from top to bottom, with one ingoing and one outgoing line belonging to pairwise the same state. The labels determine the indices of the irreducible block, e.g., $\mathcal{W}_{m_1 m_2 l}(t)$. The line attached to the clamp and leaving to the left is associated with a Kronecker delta function of the states the line connects.

FIG. 11. An example diagram for a second-order hopping process between an electrode and the molecule. It is evaluated in Appendix A.

A phonon line connecting two circles both associated to a state (site) m has a value

$$F_m^\zeta(t_i - t_j) = \exp\{\zeta A_m(t_i - t_j)\} - 1, \quad \text{with}$$

$$A_m(t) = \sum_\alpha \left(\frac{\lambda_{\alpha m}}{\omega_\alpha} \right)^2 \frac{\cos(\omega_\alpha[t + i\hbar\beta/2])}{\sinh(\hbar\omega_\alpha\beta/2)},$$

where the circle at time t_i is later on the contour than the circle at time t_j. The factor ζ is determined by the type of circles the line connects. If the circles are different $\zeta = +1$, otherwise $\zeta = -1$.

(1) Multiply with a factor $(-1)^{M+N}$, where M is the number of intersections of fermion lines on the *outside* of the contour (tunneling lines) and N is the number of intersections of fermion lines on the *inside* of the contour.

(2) We integrate over all internal times t_i (except t_1 and t_2) and sum over all electrode states ν and all internal molecule states i, j, *except* the states associated with the clamp.

As an example Fig. 11 shows a second-order diagram for a hopping process between molecule and metallic electrode. Following the rules listed above the value of this diagram is

$$\mathcal{W}_{m_1, l} = (-1)(-i)^2 |t^r|^2 \delta_{m_1 l} \mathcal{K}_l^2 \sum_\nu f_\nu e^{-i(\tilde{\epsilon}_l - \epsilon_\nu)(t_1 - t_2)} F_l^+(t_1 - t_2)$$

$$= \Gamma^r \delta_{m_1 l} \mathcal{K}_l^2 \int \frac{dE}{2\pi\hbar} f_r(E) F_l^+(\tilde{\epsilon}_l - E).$$

The last line is valid in the wideband limit with $\Gamma^{L,R} \propto \rho_e |t^{L,R}|^2$.

APPENDIX B: DETERMINATION OF THE CORRELATION FUNCTION

The correlation function with which the irreducible block is convoluted can be easily constructed from the diagrams. Lines leaving the block correspond to creation operators, lines entering the block correspond to destruction operators. The order of operators from left to right in the correlation functions corresponds to the order of the lines leaving/entering the diagram from bottom to top.

For example, let us consider some irreducible block $\mathcal{W}_{m_1 m_2 m_3 l}(t)$ which has the following order of the terminals at the left of the diagram from bottom to top: m_3 outgoing, m_2 ingoing, m_3 ingoing, m_1 outgoing, m_2 outgoing, and m_1 ingoing. Thus this rate will be convoluted with the third-order correlation function,

$$\langle U^{\dagger}_{\tilde{H}_0}(0) a^{\dagger}_{m_3} a_{m_2} a_{m_3} a^{\dagger}_{m_1} a^{\dagger}_{m_2} a_{m_1} U_{\tilde{H}_0}(0) \rangle_{\tilde{H}} = \rho_{m_1 m_3} - \rho_{m_1 m_2 m_3}.$$

APPENDIX C: VIBRATIONAL OPERATOR PRODUCTS

In the perturbation expansion of the single-particle density matrix $\rho_l(t) = \langle a^{\dagger}_l(t) a_l(t) \rangle_{\tilde{H}}$ to order n in the perturbative Hamiltonian $\tilde{H}'$ [Eq. (5)], one obtains up to n vibrational operators (equal number of χ and $\chi^{\dagger}$) at different times which act upon the same vibrational states,

$$\langle \chi_k(t_1) \chi^{\dagger}_k(t_2) \chi_k(t_3) \cdots \chi^{\dagger}_k(t_n) \rangle_{H_0}$$
$$= \left(\exp\left\{ -\frac{1}{2} \sum_{\alpha} \left(\frac{\lambda_{k\alpha}}{\Omega_{k\alpha}} \right)^2 (2N(\Omega_{k\alpha}) + 1) \right\} \right)^n$$
$$\times \exp\{\{\zeta_{12} A_k(t_1 - t_2)\} + T_C\{\zeta_{13} A_k(t_1 - t_3)\}$$

$$+ T_C\{\zeta_{3,n} A_k(t_3 - t_n)\} + \cdots\},$$

where

$$\zeta_{ij} = \begin{cases} +1 & \text{when } \chi_k(t_i) \chi^{\dagger}_k(t_j) \text{ or } \chi^{\dagger}_k(t_j) \chi_k(t_i), \\ -1 & \text{when } \chi_k(t_i) \chi_k(t_j) \text{ or } \chi^{\dagger}_k(t_i) \chi^{\dagger}_k(t_j). \end{cases}$$

The expression T_C in $T_C\{\zeta_{12} A_k(t_1 - t_2)\}$ ensures, that t_1 is later on the contour than t_2 and $A_k(t_1 - t_2)$ is given by

$$A_k(t_1 - t_2) = \sum_{\alpha} \left(\frac{\lambda_{k\alpha}}{\omega_{k\alpha}} \right)^2 \frac{\cos(\omega_{k\alpha}[t_1 - t_2 + i\hbar\beta/2])}{\sinh(\hbar\omega_{k\alpha}\beta/2)}.$$

For a correlator with n operators χ_k and $\chi^{\dagger}_k$ acting on the same state one gets $N = \frac{(n)(n-1)}{2}$ different terms $A_k(t_i - t_j)$ in the exponential function. This is due to the various operator commutations involved in deriving the above expression.

[1] K. H. Yoo, D. H. Ha, J. O. Lee, J. W. Park, J. Kim, J. J. Kim, H. Y. Lee, T. Kawai, and H. Y. Choi, Phys. Rev. Lett. **87**, 198102 (2001).

[2] T. Shigematsu, K. Shimotani, C. Manabe, H. Watanabe, and M. Shimizu, J. Chem. Phys. **118**, 4245 (2003).

[3] S. H. Choi, B. Kim, and C. D. Frisbie, Science **320**, 1482 (2008).

[4] S. Kubatkin, A. Danilov, M. Hjort, J. Cornil, J. Brédas, N. Stuhr-Hansen, P. Hedegård, and T. Bjørnholm, Nature (London) **425**, 698 (2003).

[5] E. A. Osorio, K. O'Neill, M. Wegewijs, N. Stuhr-Hansen, J. Paaske, T. Bjørnholm, and H. S. J. van der Zant, Nano Lett. **7**, 3336 (2007).

[6] M. Galperin, M. A. Ratner, and A. Nitzan, J. Chem. Phys. **121**, 11965 (2004).

[7] A. S. Alexandrov and A. M. Bratkovsky, J. Phys.: Condens. Matter **19**, 255203 (2007).

[8] A. S. Alexandrov and A. M. Bratkovsky, arXiv:cond-mat/0603467 (unpublished).

[9] A. Mitra, I. Aleiner, and A. J. Millis, Phys. Rev. Lett. **94**, 076404 (2005).

[10] Y. A. Berlin, A. L. Burin, and M. A. Ratner, J. Am. Chem. Soc. **123**, 260 (2001).

[11] B. B. Schmidt, M. H. Hettler, and G. Schön, Phys. Rev. B **77**, 165337 (2008).

[12] H. Böttger and V. V. Bryksin, *Hopping Conduction in Solids* (Akademie Verlag, Berlin, 1985).

[13] H. Park, J. Park, A. K. L. Lim, E. H. Anderson, A. P. Alivisatos, and P. L. McEuen, Nature (London) **407**, 57 (2000).

[14] H. Grabert and M. H. Devoret, *Single Charge Tunneling*, NATO Advanced Studies Institute Series Vol. 294 (Plenum, New York, 1992).

[15] J. König, J. Schmid, H. Schoeller, and G. Schön, Phys. Rev. B **54**, 16820 (1996).

[16] M. H. Hettler, W. Wenzel, M. R. Wegewijs, and H. Schoeller, Phys. Rev. Lett. **90**, 076805 (2003).

[17] A. A. Odintsov, Sov. Phys. JETP **67**, 1265 (1988).

[18] H. Haug and A. Jauho, *Quantum Kinetics in Transport and Optics of Semiconductors* (Springer-Verlag, Berlin, 1996).

[19] J. Rammer and H. Smith, Rev. Mod. Phys. **58**, 323 (1986).

[20] O. V. Konstantinov and V. I. Perel, Sov. Phys. JETP **12**, 142 (1961).

[21] H. Böttger, V. V. Bryksin, and F. Schulz, Phys. Rev. B **48**, 161 (1993).

[22] H. Böttger and V. V. Bryksin, Phys. Status Solidi B **71**, 93 (1975).

[23] H. Böttger and V. V. Bryksin, Phys. Status Solidi B **78**, 9 (1976).

[24] R. G. Endres, D. L. Cox, and R. R. P. Songh, Rev. Mod. Phys. **76**, 195 (2004).

[25] K. Senthilkumar, F. C. Grozema, C. Fonseca Guerra, F. M. Bickelhaupt, F. D. Lewis, Y. A. Berlin, M. A. Ratner, and L. D. A. Siebbeles, J. Am. Chem. Soc. **127**, 14894 (2005).

[26] S. S. Alexandre, E. Artacho, J. M. Soler, and H. Chacham, Phys. Rev. Lett. **91**, 108105 (2003).

[27] E. M. Conwell and S. Rakhmanova, Proc. Natl. Acad. Sci. U.S.A. **97**, 4556 (2000).

[28] P. Henderson, D. Jones, G. Hampikian, Y. Kan, and G. Schuster, Proc. Natl. Acad. Sci. U.S.A. **96**, 8353 (1999).

[29] A. Joy, G. Guler, S. Ahmed, L. W. McLaughlin, and G. B. Schuster, Faraday Discuss. **131**, 357 (2006).

[30] G. P. Triberis, C. Simserides, and V. C. Karvolas, J. Phys.: Condens. Matter **17**, 2681 (2005).

[31] G. P. Triberis and M. Dimakogianni, J. Phys.: Condens. Matter **21**, 035114 (2009).

[32] E. B. Starikov, Philos. Mag. **85**, 3435 (2005).

[33] J. Olofsson and S. Larsson, J. Phys. Chem. B **105**, 10398 (2001).